AIAA 80-1127R

MHD Measurement of Acoustic Velocities in Rocket Motor Chambers

Michael M. Micci* and Leonard H. Caveny†
Princeton University, Princeton, N.J.

A linear analysis of longitudinal acoustic waves (either forced or self-induced) at or near the fundamental frequency in solid rocket chambers revealed that the acoustic velocity phase angle relative to the head-end pressure at the chamber midpoint is strongly dependent on the real part of the overall pressure-coupled response function and the imaginary part of the overall velocity-coupled response function. A flowmeter based on Faraday's Law was devised to demonstrate the feasibility of such velocity measurements under rocket motor conditions. The interaction of an externally-excited magnetic field with the unsteady velocity of high-temperature combustion gases results in a corresponding unsteady electrical potential whose magnitude is proportional to the flow velocity. The system is readily calibrated since electrical output does not depend on knowledge of ionization level and electrical conductivity (within certain limits) and measurements are independent of propellant type. Motor firing data has been used to deduce the real part of the pressure-coupled response from the phase angles between head-end pressures and midpoint velocities and the imaginary part of the velocity-coupled response from the phase angles between head- and nozzle-end pressures. The overall response functions measured in the device are compatible to the form used in stability prediction models.

Nomenclature

B = magnetic flux density, webers/m^2
E = electric field strength, V/m
l = length, m
L = electrode separation, m
p = pressure, Pa
R_p = pressure-coupled response function
R_v = velocity-coupled response function
S = area, m^2
t = time, s
U = velocity, m/s
V = potential, V
α = flowmeter coefficient
ϕ = phase angle, deg

Superscripts

$()'$ = fluctuating quantity
$\bar{()}$ = mean quantity

Introduction

CONSIDERABLE attention has been given to investigating methods of obtaining solid propellant pressure- and velocity-coupled burning rate response functions.[1] All methods require careful interpretation of data and are subject to a wide range of uncertainties. The measured response functions are device dependent, particularly the velocity-coupled response which is a function of local mean flow velocity, unsteady velocity amplitude, and details of the boundary layer.[2] In the case of a rocket motor experiencing a longitudinal oscillation, the burning propellant is subjected to simultaneous velocity and pressure oscillations which cover a range of amplitudes and phases. Many investigations have attempted to devise experiments which subject propellants to either well-defined (sinusoidal) pressure oscillations or well-defined velocity oscillations. With the exception of the microwave pressure-coupled burning rate measurements,[3] establishing the relationship between the simple forcing function and the burning rate response requires a rather complete understanding of the flowfield. This paper introduces a new development in an approach that deals with the overall propellant responses within a rocket motor chamber. The approach obtains both overall pressure- and velocity-coupled burning rate responses using data reduction procedures which are inverses of widely used stability prediction techniques.[4] Accordingly, when the results are used for predictions a portion of the errors are compensated for.

The forced longitudinal wave (FLW) motor is a high loading density subscale solid propellant rocket motor containing a center perforated grain.[5,6] Low amplitude longitudinal oscillations are excited by periodically interrupting the outflow through a sonic nozzle. Through the use of a linear analysis, dynamic pressure measurements at the head and nozzle ends of the solid propellant grain have been used to deduce the real and imaginary parts of the propellant velocity-coupled burning rate response.[6] The pressure-coupled response is the other required input for a stability prediction. Indeed, it is desirable to obtain the pair in a single experiment. A method for making dynamic velocity measurements inside the rocket motor chamber by utilizing a magnetic velocimeter was recently suggested by Glick et al.[8] This paper describes the development and adaptation of a velocimeter for a dynamic velocity measurement inside the FLW motor and the use of the previously developed linear analysis to deduce propellant response functions from the data.

Analysis

A linear analysis where terms of the order of the Mach number squared and higher are neglected was developed to model the nonsteady and steady flow characteristics of the FLW motor.[6] The analysis includes both pressure and velocity coupling along with flow turning losses and erosive burning. The form of the response functions utilized in the

Presented as Paper 80-1127 at the AIAA/SAE/ASME 16th Joint Propulsion Conference, Hartford, Conn., June 30-July 2, 1980; submitted Dec. 29, 1980; revision received Sept. 8, 1981.

*Ph.D. Candidate, Mechanical and Aerospace Engineering Dept.; currently, Assistant Professor, Aerospace Engineering Dept., The Pennsylvania State University. Member AIAA.

†Senior Professional Staff Member, Mechanical and Aerospace Engineering Dept.; currently at AFOSR/NA, Bolling AFB, Washington, D.C. Associate Fellow AIAA.

analysis contains terms describing both the burning rate and the nonisentropic flame temperature responses. The analysis has been used to deduce the real and imaginary parts of the overall velocity-coupled responses of propellants within the rocket motor. This was made possible when the analysis demonstrated that the structure of the steady-state standing pressure wave as measured at the pressure antinodes is a strong function of the velocity-coupled response and a weak function of the pressure-coupled response. The analysis also indicated that the structure of the pressure node is a strong function of both the pressure-coupled and velocity-coupled propellant responses. Thus an accurate pressure measurement at the nodal point can be utilized to deduce the propellant pressure-coupled response. The type of multipoint pressure instrumentation required to obtain an accurate measurement at the pressure node has been shown by work on the solid propellant impedance tube.[9] However, measurement of the fundamental mode standing wave structure at the pressure node is difficult inside a rocket motor since multipoint pressure instrumentation which requires the drilling of pressure ports through the propellant grain would disturb the flow processes.

The linear analysis assessed what information concerning the propellant response functions could be gained by measurements of the acoustic velocities at the midpoint of the chamber where $u'/\bar{u}$ is a maximum. The analysis revealed that the amplitude of the velocity oscillation is a strong function of both the imaginary part of the pressure-coupled response and the real part of the velocity-coupled response.[7] The phase of the velocity oscillation relative to the head-end pressure oscillation was found to be a strong function of both the real part of the pressure-coupled response and the imaginary part of the velocity-coupled response. Since the velocity-coupled response can be deduced solely from pressure measurements taken from previous experiments, the amplitude and phase of the acoustic velocity can be utilized to deduce the real and imaginary parts of the pressure-coupled response. Figure 1 shows the pronounced effect the real part of the pressure-coupled response has on the acoustic velocity standing wave phase angle while the remaining motor parameters such as velocity-coupled response, frequency, and motor length are kept constant. At the flowmeter location near the chamber midpoint, a change in the real part of the pressure-coupled response (as defined by Ref. 6) from a value of 0 to 6 produces a measurable phase angle change of approximately 13 deg. The acoustic velocity amplitude as a function of distance down the port as calculated by the linear analysis is shown in Fig. 2. When the imaginary part of the pressure-coupled response is varied from a value of -3 to $+3$ the amplitude of the velocity oscillation at the flowmeter location varies by only 15%. The purpose of these experiments was the deduction of the pressure-coupled real part and the velocity measurements were taken to obtain the phase angle between head-end pressure and midpoint velocity. Thus, the accuracy of the velocity amplitude was not a primary factor. Since the flowmeter calibration (described in the following section) was obtained at flow velocities much less than the oscillatory flow velocities and, therefore, had to be extrapolated, sufficient accuracy was not obtained in the measurement of the oscillatory velocity amplitude to permit the deduction of the imaginary part of the pressure-coupled response. However, this component of the propellant response is not required for stability calculations.[4] Phase angle measurements do not require amplitude calibrations. The phase and amplitude of the midpoint velocity were found to be nearly linear functions of the real and imaginary parts, respectively, of the pressure-coupled response; while the phase angle is a weak function of the imaginary part and the amplitude is a weak function of the real part of the pressure-coupled response. Thus, when sufficiently accurate acoustic velocity phase angle measurements are made, the real part of the pressure-coupled response within the motor can be

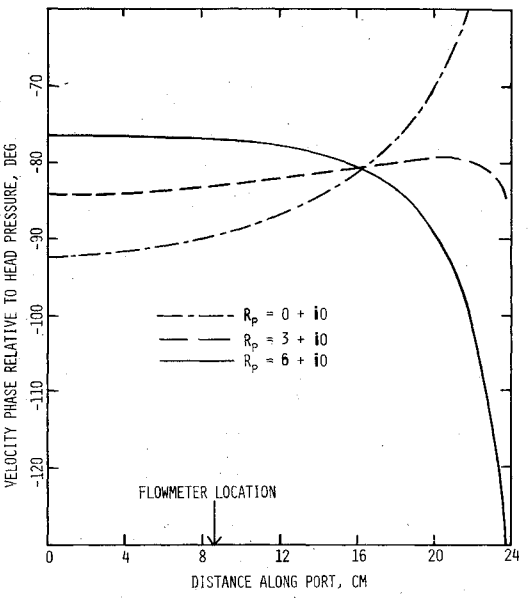

Fig. 1 Phase angle of velocity oscillation relative to head-end pressure oscillation as a function of port distance. Changes in the real part of the pressure-coupled response produce measurable changes in the phase angle at the chamber midpoint and elsewhere.

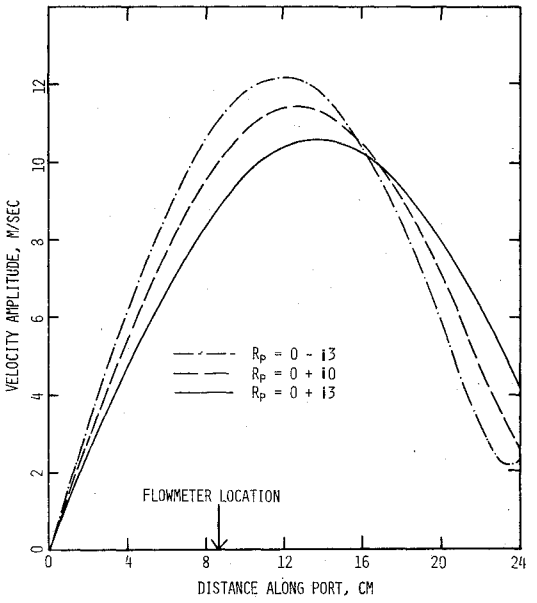

Fig. 2 Amplitude of the velocity oscillation as a function of port distance showing changes in the imaginary part of the pressure-coupled response produce measurable changes in the acoustic velocity amplitude at the chamber midpoint.

deduced. Table 1 summarizes the dependence of the four observables within the rocket motor chamber to the four response function components. One can discern from Table 1 that the two response function components which are easiest to deduce, the real part of the pressure-coupled response and the imaginary part of the velocity-coupled response, are the two components necessary for stability calculations.

We are aware that the idealized one-dimensional flow equations do not account for the unsteady effects of radial velocity profiles in the chamber (see Ref. 10 for a discussion). The governing equations for the linear analysis were rederived following Ref. 9 taking into account representative viscous radial velocity profiles. It was found that for a turbulent flow profile which is expected to exist over 80% of the port of the

Table 1 Dependence of rocket motor observations on response functions

Observable	Ease of measurement	$R_{p_{real}}$	$R_{p_{imag}}$	$R_{v_{real}}$	$R_{v_{imag}}$
$\phi_{u'_{mid}-p'_{head}}$	Relatively easy	Strong	Weak	Weak	Strong
$\phi_{p'_{noz}-p'_{head}}$	Relatively easy	Weak	Weak	Weak	Strong
u'_{mid}/p'_{head}	Requires accurate calibration	Weak	Strong	Strong	Weak
p'_{noz}/p'_{head}	Requires accurate calibration	Weak	Weak	Strong	Weak

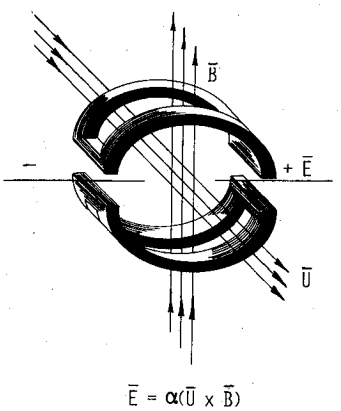

Fig. 3 Principle of operation of magnetic flowmeter. Induced electric field is proportional to both flow velocity and magnetic field intensity.

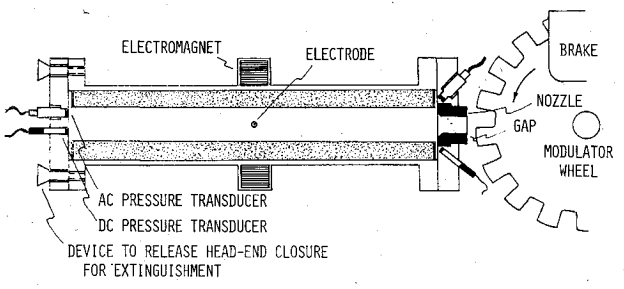

Fig. 4 Magnetic flowmeter installed in forced longitudinal wave (FLW) motor showing proximity of magnetic field excitation coils to solid propellant grain.

rocket motor the greatest error is incurred in the deduction of the imaginary part of the velocity-coupled response and that the magnitude of this response function error is less than 0.3. Thus the reservations[11] concerning the adequacy of the widely used one-dimensional unsteady flow procedures (e.g., Refs. 1 and 4) do not detract from the accuracy of obtaining pressure- and velocity-coupled response functions within the framework of a specific linearized unsteady flow model.

MHD Flowmeter

The flowmeters developed for this investigation operate according to Faraday's Law, which states that a conductor moving in a magnetic field will have an induced electromotive force proportional to the rate at which the magnetic field lines which are steady with time are being passed. Faraday's Law is derivable from Maxwell's Equation

$$\nabla \times E = -\frac{\partial B}{\partial t} \tag{1}$$

Taking the surface integrals of both sides of the equation

$$\int (\nabla \times E) \cdot dS = -\int \frac{\partial B}{\partial t} \cdot dS \tag{2}$$

Applying Stokes' theorem to the left side of the equation one obtains

$$\int E \cdot dl = -\int \frac{\partial B}{\partial t} \cdot dS \tag{3}$$

The electromotive force (emf) is defined to be

$$\text{emf} = \int E \cdot dl \tag{4}$$

Thus,

$$\text{emf} = -\frac{\partial}{\partial t} \int B \cdot dS \tag{5}$$

Assuming that the resistance of the moving conductor is much less than that of a voltage measuring device, the voltage measured across the moving conductor is equal to the electromotive force. Thus

$$V = -UBL \tag{6}$$

where V is the voltage, U the velocity of the moving conductor (m/s), B the magnetic flux density (webers/m^2), and L the electrode separation (m). This is shown schematically in Fig. 3.

Noting prevents the moving conductor from being a fluid. Upon inspection of the preceding equations one can see that the measured voltage is not a function of the conductivity; however, this is true only within certain limits. The conductivity must not be of such large extent that magnetohydrodynamic forces distort the velocity profile. This situation can occur with the flow of liquid metals. On the other hand, there is a minimum conductivity (approximately 10^{-3} mhos/m) below which the resistance of the voltage measuring device becomes of the same order as the moving conductor and the output begins to drop. In the case of nonionized gases, the output is effectively zero. MHD flowmeters have been used to measure the fluid flow velocities for common liquids, slurries, liquid metals in nuclear reactors, ionized plasmas, and blood flow in veins and arteries.[12] It has been shown[12] that the result of Eq. (6) is valid when the fluid velocity profile is axisymmetric, in which case the velocity U is the mass-averaged mean over the flow cross section.

The frequency response of the MHD flowmeter has no inherent limitations. One inherent loss mechanism is that current flow between the electrodes will introduce ohmic losses. Indeed operation while drawing substantial current is the principle of the MHD generator where energy is extracted from the moving flow. Insulating the walls containing the flow and a large instrument input impedance maintains the desired low current flow. However, when the magnetic field intensity varies along the axis of the pipe (which it must do for any field producing device of finite size) the phenomenon of "end-shorting" arises. The induced electromagnetic force varies along the axis of the flow causing currents to circulate in the fluid and lowering the voltages measured at the electrodes. This modifies Eq. (6) by the insertion of a

multiplicative constant

$$V = -\alpha UBL \tag{7}$$

where α is less than unity. If the exact axial variation of the magnetic field is known then the effect of end-shorting can be calculated and taken into account.[13] However for a laboratory device, geometric complexities make this very difficult and an in situ calibration can be utilized to measure α by simply measuring the output voltage V as a function of a known fluid flow rate U.

A few examples exist in the literature of the application of a MHD flowmeter to the measurement of a rocket exhaust velocity.[14,15] Both studies involved the measurement of the supersonic exhaust velocities at the exit plane of a converging-diverging nozzle. Holme[14] analyzed the performance of the flowmeter for several liquid propellant combinations and obtained favorable results with all but the hydrogen peroxide monopropellant due to its low flame temperature. The device utilized an alternating magnetic field, an excitation procedure which is also utilized in most liquid MHD flowmeters. This is done to remove the dc effects of polarization. Both sine and square wave excitation have been used in flowmeters. The amplitude of the alternating induced voltage is thus proportional to the flow velocity.

The performance of the flowmeter adapted to the measurement of unsteady velocities of the order of 10 m/s was analyzed. An analysis applied the Biot-Savart law to calculate the magnetic flux density inside several air core coil configurations which could fit around the phenolic liner within which the propellant grains are cast. The analysis showed that air core coils which were shaped to fit around the phenolic liner but sufficiently small to fit inside the forced longitudinal wave (FLW) motor pressure vessel (Fig. 4) could generate a magnetic field intensity on the order of 100 G, the same magnitude obtained by Holme in his device.

A square wave magnetic field excitation was chosen due to the ease of data reduction. When an alternating magnetic field is used, induced voltages appear in the electrode circuitry and must be subtracted from the electrode output to obtain the flow signal. A sine wave excitation induces a sine wave voltage while a square wave excitation induces a voltage only when the field is reversed. Thus, while the magnetic field strength is constant there is no induced voltage in the electrode circuit. The inductance of the air core coil was calculated and found to be sufficiently low to have negligible effect on the reversing of the magnetic field. An electronic device was designed and built to accept the output of a dc power supply and to switch the polarity at a user selected frequency to obtain a square wave output.

The propellant selected for testing inside the FLW motor is a composite propellant consisting of 86.5% trimodal ammonium perchlorate and 13.5% HTPB. The propellant formulation and properties are listed in Table 2. This is a high-energy propellant which can experience combustion fed acoustic instabilities. It has been shown that the predominant source of free electrons in the combustion products of solid propellants is the thermal ionization of trace amounts of alkali metal impurities, principally sodium and potassium.[16] The presence of 10 ppm of sodium, for instance, can dramatically increase the theoretical conductivity of propellant combustion products. The amounts of these impurities in the ingredients of various solid propellants were measured in Refs. 16 and 17 and found to be approximately 100-200 ppm of sodium and 25-300 ppm of potassium. Experimental measurements of the electrical conductivity of the combustion products of several solid propellants at both atmospheric and chamber pressures are reported in Refs. 17 and 18 and in all instances the measured conductivities are greater than 10^{-3} mhos/m. Thus sufficient flow conductivity for a range of solid propellant formulations is assured.

Table 2 Propellant formulation and properties

Formulation, %		
Binder, HTPB		13.5
Ammonium perchlorate		86.5
45 μm	20	
180 μm	20	
400 μm	60	
Density, g/cm^3		1.68
Strand burning rate		
at 6.9 MPa, cm/s		0.84
Exponent		0.60

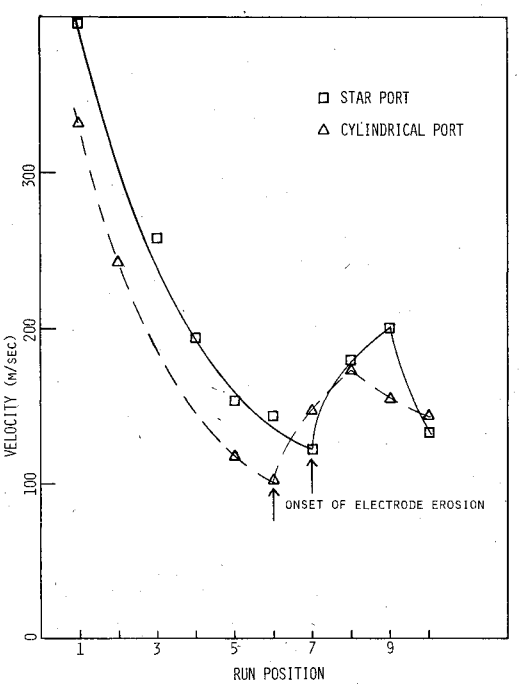

Fig. 5 Chamber midpoint mean velocity as a function of time. The effect of electrode erosion can be seen in the latter portion of each motor run.

The coils selected for use in the flowmeter consist of two coils of 100 turns each of number 26 enameled copper wire. The coils were wound on 3.5×1.5 cm forms and curved to conform to the soild propellant phenolic liner. A stainless steel pressure vessel surrounds the coils but was found to have negligible effect on the field interior to the electromagnets due to its low (1.02) relative magnetic permeability, a quantity which gives the ratio of which the magnetic field lines prefer the material to air. The interior magnetic field intensity was mapped using a gaussmeter. It was found that the addition of iron cores to the electromagnets increased the magnetic field integrated over the flow area by a factor of two. Thus the inductance, which is proportional to the enclosed flux divided by the applied current, increased by no more than a factor of two and the frequency response of the field reversal would not be impaired. Thus the addition of the cores doubled the velocity signal without requiring additional electrical power for the electromagnets. Later firings of the FLW motor with the flowmeter were conducted with the air core electromagnets placed outside of the stainless steel pressure vessel. This was done to decrease their rate of corrosion due to the hydrochloric acid contained in the propellant combustion products. The decrease in magnetic field strength due to the increased distance between the coils was compensated for by an increase in the supplied amperage.

The output of the electrodes was connected to a 100 Mohm input impedance amplifier with a user selectable gain of between 10 and 100. The dynamic range of the unsteady

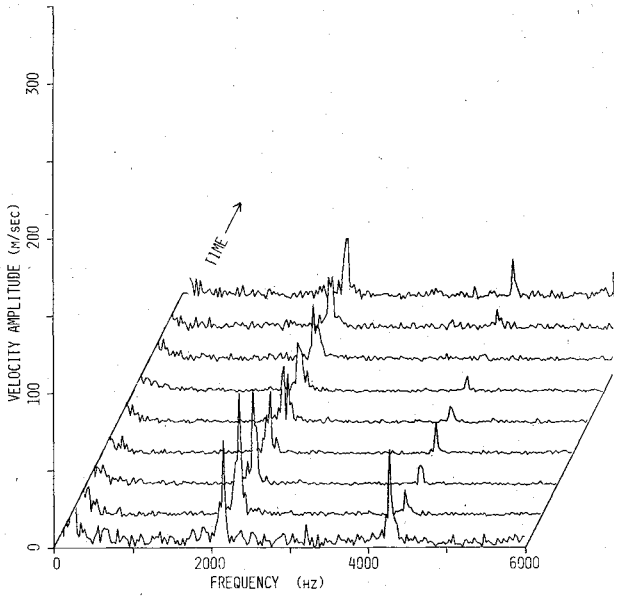

Fig. 6 Acoustic velocity amplitude spectra as a function of time showing motor excitation frequency of 2100 Hz above background noise.

velocity component was peaked to obtain effective use of the 12 bit digitizing word. End-to-end calibration confirmed that the electronic phase angle errors had been reduced to less than 0.1 deg. The digitized signals were stored for subsequent digital spectal analysis. The mass flow rate of the flowmeter was calibrated with a saline solution flow while situated within the motor pressure vessel. Even though the flowmeter was calibrated with a liquid, the calibration will be valid for any gas or liquid having sufficient conductivity provided the flow profile is axisymmetric. The flowmeter output was found to be linear over the range of flow velocities obtainable.

Experimental Results

A series of solid propellant motors were fired using the flowmeter. The polarity of the magnetic field was switched at 10 Hz in order to measure the mean velocity at approximately ten times during the motor firing. The unsteady acoustic velocity data were taken continuously during the experiment. The first part of Fig. 5 shows the mean velocity decreasing as the chamber cross-sectional area increases. The abrupt velocity increase is attributed to a section of the molybdenum electrodes breaking away. Since the flowmeter output is proportional to the electrode spacing, any loss of material from the ends of the electrodes will cause a voltage increase for a given flow velocity. The calibration based on the initial electrode separation was applied to all the velocity data obtained. The mean velocity for the star port motor will not be accurate due to nonaxisymmetric flow. However, the error will diminish with motor run time as the port approaches a cylindrical geometry. The use of tungsten electrodes 1.6 mm in diameter eliminated the electrode damage problem in later firings. No mean flow data were taken during subsequent tests because the data acquisition was optimized to obtain high-quality unsteady velocity measurements. As shown in Fig. 6, the unsteady velocity amplitude spectra vary slowly as a function of time. The nine spectral calculations shown cover a total time period of 0.5 s. This motor was excited at 2100 Hz and the velocity oscillation at that frequency can be observed clearly. As expected during most of the motor firing very little second harmonic content exists due to the proximity of the flowmeter electrodes to the second harmonic velocity node. The low frequency activity is a direct result of changing polarization effects and electrode erosion. However, very little interharmonic noise was observed and the digital

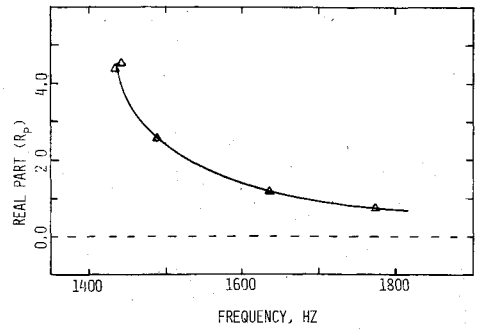

Fig. 7 Deduced real part of the pressure-coupled response as a function of frequency at a pressure of 5.5 MPa showing characteristic response function peak.

spectral analysis was utilized effectively to compute the phase angle between the midpoint velocity oscillation and the head-end pressure oscillation. Since the forcing frequency was accurately known from the pressure measurements, the frequency interval was increased to improve the amplitude and phase resolution, i.e., frequency averaging was implemented.[19] Additional accuracy was obtained through an increase in the sampling time, i.e., ensemble averaging. The error associated with the phase angle measurement was quantified by the digital spectral coherence function. The error in the phase angle measurement was reduced to less than ± 1.8 deg with a 95% confidence factor.

In conjunction with the unsteady pressure measurements made at the head and nozzle ends of the FLW motor (gain and phase transfer functions), the midpoint velocity phase angle was utilized to deduce the real part of the pressure-coupled response through the use of the linear analysis. Through an iterative procedure a unique set of values for the real part of the pressure-coupled response and the real and imaginary parts of the velocity-coupled response were found which, when substituted in the linear analysis, reproduced the measured oscillating pressures and velocities. Figure 7 shows the deduced real part of the pressure-coupled response as a function of frequency from five firings of the FLW motor at approximately 5.5 MPa chamber pressure. Run-to-run agreement was obtained. The measured response function is consistent with our current understanding of pressure-coupled response function behavior. The values for the real and imaginary parts of the velocity-coupled response, which were obtained simultaneously, follow the results published in Ref.6.

Conclusions

A flowmeter based on Faraday's Law is being utilized to measure both mean and unsteady velocities within the ports of centrally perforated solid propellant rocket motors. A linear analysis demonstrated that measurements of the midsection acoustic velocity and phase angle would permit the deduction of the real and imaginary parts of the pressure-coupled response. Measurements of the acoustic phase angles have been obtained and results have been used to deduce the real part of the pressure-coupled response for an AP/HTPB propellant from 1400-1800 Hz at approximately 5.5 MPa. The experimental and analytical developments presented in this paper coupled with those of Ref. 6 will permit both real and imaginary parts of the overall pressure-coupled and velocity-coupled response functions to be deduced. One of the many features of the techniques is that response functions are obtained under rocket motor conditions. The oscillations can be either intrinsic or externally excited.

Acknowledgments

This research was sponsored by the Air Force Office of Scientific Research under grant AFOSR-76-3104. Fabrication of the apparatus, preparation of propellants, and specialized

electronics were ably performed by C. R. Felsheim, S. O. Morris, and L. M. Pokrocos. Specialized magnetic field measurement equipment was provided by Duncan MacArthur. The encouragement of Robert L. Glick in the development of a flowmeter based on Faraday's Law and the thermochemistry calculations by Robert S. Brown are gratefully acknowledged.

References

[1] Brown, R. S., Culick, F.E.C., and Zinn, B. T., "Experimental Methods for Combustion Admittance Measurements," *Progress in Astronautics and Aeronautics: Experimental Diagnostics in Combustion of Solids*, Vol. 63, AIAA, New York, 1978, pp. 191-220.

[2] Price, E. W., "Velocity Coupling in Oscillatory Combustion of Solid Propellants," *AIAA Journal*, Vol. 17, July 1979, pp. 799-800.

[3] Strand, L. D., Magiawala, K. R., and McNamara, R. P., "Microwave Measurement of the Solid Propellant Pressure-Coupled Response Function," AIAA Paper 79-1211, June 1979.

[4] Lovine, R. L., "Standardized Stability Prediction Method for Solid Rocket Motors," Air Force Rocket Propulsion Laboratory, AFRPL-TR-76-32, May 1976.

[5] Micci, M. M., Caveny, L. H., and Summerfield, M., "Solid Propellant Rocket Motor Responses Evaluated by Means of Forced Longitudinal Waves," AIAA Paper 77-974, July 1977.

[6] Micci, M. M., Caveny, L. H., and Sirignano, W. A., "Linear Analysis of Forced Longitudinal Waves in Rocket Motor Chambers," *AIAA Journal*, Vol. 19, Feb. 1981, pp. 198-204.

[7] Micci, M. M., "Solid Propellant Response Functions Deduced by Means of Forced Longitudinal Waves in Rocket Motors," Ph.D. Thesis, Princeton University, Princeton, N.J., April 1981.

[8] Glick, R. L., Herren, K. A., and Hessler, R. O., "Alternate Approaches to Measurement of Nonsteady Properties," AIAA Paper 79-0163, Jan. 1979.

[9] Zinn, B. T., Daniel, B. R., and Baum, Y. D., "Experimental Determination of Solid Propellant Admittances by the Impedance Tube Method," AIAA Paper 80-0281, Jan. 1980.

[10] Celmins, A., "Modified Governing Equations for Unsteady Compressible Flow in Ducts," *Journal of Applied Mechanics*, Vol. 45, Dec. 1978, pp. 723-726.

[11] Glick, R. L., personal communication, June 10, 1980.

[12] Shercliff, J. A., *Theory of Electromagnetic Flow-Measurement*, Cambridge University Press, Cambridge, England, 1962.

[13] Boucher, R. A. and Ames, D. B., "End Effect Losses in dc MHD Generators," *Journal of Applied Physics*, Vol. 32, May 1961, pp. 755-759.

[14] Holme, J. C., "Investigation of an Electromagnetic Technique for the Independent Measurement of Chemical Rocket Exhaust and Vector," Astrosystems International, Inc., Fairfield, N.J., AFFDL-TR-65-98, June 1965.

[15] Graham, A. R., "Transient and Steady State Measurement of Rocket Engine Performance," General Electric, Malta, N.Y., New York State ASDA 64-103, Oct. 1964.

[16] Smoot, L. D., "Measurement and Prediction of Microwave Attenuation in the Near-Regions of Solid Propellant Rocket Exhaust Plumes with Application to Proposed Sprint Propellants," *Bulletin of the 20th Interagency Solid Propulsion Meeting*, Chemical Propulsion Information Agency Publ. 49B, Oct. 1964, pp. 131-174.

[17] Bestgen, R. F., "A Study of the Effects of Electric Fields on Solid Propellant Burning Rates," AFRPL-TR-71-87, July 1971.

[18] Capener, E. L., Chown, J. B., Dickinson, L. A., and Nanevicz, J. E., "Studies on Ionization Phenomena Associated with Solid-Propellant Rockets," *AIAA Journal*, Vol. 4, Aug. 1966, pp. 1349-1354.

[19] Otnes, R. K. and Enochson, L., *Applied Time Series Analysis, Basic Techniques*, Vol. 1, John Wiley and Sons, New York, 1978.